Eur. J. Wood Prod. (2015) 73:17–27
DOI 10.1007/s00107-014-0851-3

ORIGINAL

Local variation of modulus of elasticity in timber determined on the basis of non-contact deformation measurement and scanned fibre orientation

Min Hu · Marie Johansson · Anders Olsson · Jan Oscarsson · Bertil Enquist

Received: 12 June 2014 / Published online: 15 October 2014

Abstract During the last decade, the utilization of non-contact deformation measurement systems based on digital image correlation (DIC) has increased in wood related research. By measuring deformations with DIC systems, surface strain fields can be calculated. The first aim of this study concerns the possibility to detect detailed strain fields along the entire length of a wooden board subjected to pure bending and the potential of using such strain fields to determine a bending modulus of elasticity (MOE) profile along a board. Displacements were measured over 12 subareas along a flat surface of the board. For each such area, a separate local coordinate system was defined. After the transformation of locally measured coordinates to a global system, high resolution strain fields and a corresponding bending MOE profile were calculated. A second method in establishing bending MOE profiles is to use fibre angle information obtained from laser scanning and a calculation model based on integration of bending stiffness over board cross sections. Such profiles have recently been utilized for accurate strength grading. A second aim of this study was to investigate the accuracy of the bending MOE profiles determined using the latter method involving fibre angle information. Bending MOE profiles determined using the two described methods agree rather well. However, for some patterns of knot clusters, the local bending MOE, calculated on the basis of fibre angles and integration of bending stiffness, is overestimated. Hence, this research adds knowledge that may be utilized to improve the newly suggested strength grading method.

M. Hu (✉) · M. Johansson · A. Olsson · B. Enquist
Department of Building Technology, Linnaeus University, Växjö, Sweden
e-mail: min.hu@lnu.se

J. Oscarsson
SP Wood Technology, SP Technical Research Institute of Sweden, Växjö, Sweden

List of symbols

E_l	MOE in the local longitudinal fibre direction
E_x	MOE in the global x-direction, i.e. the direction of the board
E_b	Average bending MOE over cross-sections along the global x-direction, also referred to as bending MOE
EI_z	Bending stiffness over cross sections with respect to the global z-direction
ε_x	Normal strain in the global x-direction
ε_y	Normal strain in the global y-direction
ε_{xy}	Shear strain in the global xy-plane

1 Introduction

Most strength grading machines on the European market are based on the relationship between a modulus of elasticity (MOE) and the bending strength of timber members. In most cases, the MOE is determined either as a flatwise bending MOE calculated as an average over a length of between 0.6 and 1.2 m, or as a global axial dynamic MOE representing an average value of the entire board. In reality, knots and other defects cause large variation in stiffness along boards and if this variation is accurately considered, better strength predictions are achieved. In many studies, a higher coefficient of determination (R^2) with respect to strength could be obtained with better knowledge of local MOE variation. For example, Orosz (1976) concluded, based on an investigation of west coast hemlock, that the prediction of tension strength could be improved by shortening the gauge length for measuring the MOE. This

means that a more localized MOE is then used as an indicating property to strength. In this context, the measurement of fibre angles from laser scanning using the tracheid effect (Nyström 2003) has shown to be a powerful tool in establishing high resolution bending stiffness profiles (Oscarsson 2014; Olsson et al. 2013). Because wood is a strongly orthotropic material, with high stiffness in the fibre direction, deviation in fibre orientation around knots, for example, causes considerable reduction of stiffness in the direction of the board. With knowledge of local fibre orientation from laser scanning and material property transformation, the corresponding stiffness in the global longitudinal axis of a wood member can be obtained; therefore, it is possible to calculate, by means of integration, a bending stiffness profile along an individual wood member. Moreover, this can be done at a speed corresponding to the production speed at sawmills, allowing it to be utilized for commercial machine strength grading purposes.

In the last decade, the utilization of non-contact deformation measurement systems based on digital image correlation (DIC) has increased in the area of wood technology research, e.g. Sjödin et al. (2006). Based on deformations measured by DIC systems, high resolution strain fields on the surfaces are calculated. Moreover, by combining the repeated DIC measurements over a number of subareas, strain fields representing large areas are established (Oscarsson 2014). In the present study, this is utilized to assess the strain fields over an entire board.

The aim of the present study was (1) to investigate the bending MOE profile along a board, established on the basis of high resolution displacement data obtained from the DIC measurements of a board subjected to bending, and (2) to compare this profile with a bending MOE profile established on the basis of fibre orientation obtained from laser scanning as suggested by Olsson et al. (2013). A 3D non-contact deformation measurement system named ARAMIS™ was employed to capture the displacements on one of the board's flat surfaces due to pure bending, while a system named TRITOP was used to relate data from separate measurements of subareas to a common, global coordinate system. The displacements were detected at prescribed bending moments and a bending MOE profile could then be established and compared with the profile based on fibre orientation information. Agreements and discrepancies between the two different profiles are discussed.

2 Materials and methods

A board of Norway spruce (*Picea abies* L. Karst.), dimensions 50 × 150 × 3,900 mm^3, was chosen for the study from a sample collected in southern Sweden. The board was chosen due to its relatively large defects/knots and distinct weak sections characterized by knot clusters. Relevant material properties are found in Table 1. Before the tests, the board was conditioned in a climate room with a temperature of 20 °C and a relative humidity of 65 %. Dynamic tests had previously been carried out on this board (Hu et al. 2011), whereby the dynamic MOE (cf. Table 1) had been registered in accordance with the first axial resonance frequency.

Table 1 Relevant material parameters of the specimen, data from Hu et al. (2011)

Material parameter	Value
Density	454 kg/m^3
1st axial frequency	637 Hz
Dynamic MOE	10.98 GPa

The laboratory measurements provided (1) 3D coordinates of one flat surface of the board during loading and (2) fibre angles on all edge and flat surfaces of the board. The test set-up and measuring procedures are further described below. In addition to the laboratory tests, the study also comprises numerical calculation and modeling using the software MATLAB®.

2.1 Displacement measurement on board subjected to pure bending

The DIC system ARAMIS, equipped with dual digital cameras, was used to observe the development of 3D deformations on one of the board's surfaces. ARAMIS recognises the pattern of the object's surface in digital images and allocates coordinates to sub-images, each consisting of a limited number of pixels. During loading, ARAMIS records digital images used to calculate strain fields of the measured surface (GOM mbH 2007). In this study, however, only displacement data from ARAMIS was utilized. Strains were calculated using self-developed routines in a MATLAB environment.

To determine a bending MOE profile based on displacements measured on one flat surface of the board, a constant and pure bending moment must be applied along the whole member. To enable such a moment, the board was lengthened by finger jointing an extra 550 mm long board at each end of the original board. The bending test was then arranged as a four-point bending, where the board was symmetrically loaded at two points 3.9 m apart; see Fig. 1a. Therefore, the mid-span, i.e. the whole original board, was exposed to a constant pure bending moment. The load was increased in five steps and for each load step images were recorded. Table 2 illustrates the corresponding load/stress levels. The stress levels in the table are the nominal maximum normal stresses in the x-direction at the edges of the board and are calculated on the basis of Euler–

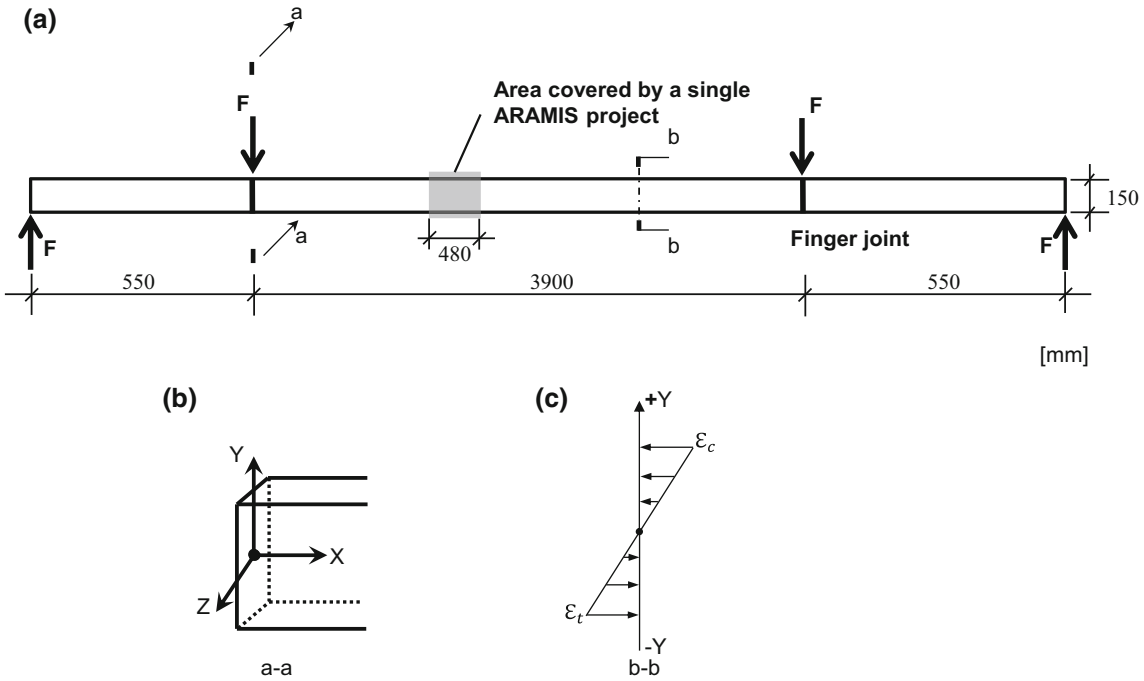

Fig. 1 Arrangement of four-point bending test is illustrated in **a**, giving a constant and pure bending moment over the whole length of the studied 3,900 mm long board. Non-contact deformation measurements were performed by implementing a number of ARAMIS projects, each covering a length of 480 mm, along the board while the load was kept constant. **b** The definition of the global coordinate system. The origin is located at the centre of the left end surface of the original board. **c** The idealized strain distribution over the cross-section '*b-b*' in accordance with the beam theory corresponding to the applied pure bending moment

Table 2 Information on the load stages of the ARAMIS measurements

Stage no.	0	1	2	3	4
Nominal load F [kN]	0.5	2.0	4.0	5.5	7.0
Nominal stress σ [MPa]	1.5	5.9	11.7	16.1	20.5
Measuring sequence	→	→	→	←	←

Arrows in the table indicate the sequence of examining the 12 ARAMIS projects

Bernoulli beam theory, assuming that the material stiffness is constant over the cross section. To record images along the whole mid-span, 12 ARAMIS projects, each covering an area of 480 × 480 mm^2 on the object surface, were created along the board. Thus the cameras were placed at twelve different positions along the board while the load was kept constant. The measurement areas covered by the ARAMIS projects were numbered as project 1 to project 12, from the left end to the right end of the board. A local coordinate system was defined for each project. In Table 2, 'Measuring sequence' indicates the sequence of examining the 12 projects at a certain load stage. A right-pointing arrow in Table 2 indicates the order of the measurements from project 1 to project 12, i.e. from left to right, whereas a left-pointing arrow indicates the measuring sequence being performed from project 12 to project 1, i.e. from right to left. If any creep occurred during the load stages, each lasting for about 15 min, it would be possible to observe it by means of the described procedure, since more creep would appear in the right end of the board for load steps 0, 1, 2 and 4 while more creep would appear in the left end of the board in load step 3.

The aim of the ARAMIS measurements was to record displacements occurring on the whole area of 150 × 3,900 mm^2 of the object surface, but due to test set-up limitations and the edge effect on both tension and compression sides of the board, part of the board surface was not captured by ARAMIS and the data points very close to the edges were therefore disregarded. Hence, only an area of about 132 × 3,710 mm^2 was actually evaluated. The resolution of the data was approximately 3 mm in both *x*- and *y*-directions. With the aid of the measurement system TRITOP, the local coordinate system of the 12 individual ARAMIS projects were each transformed to a global

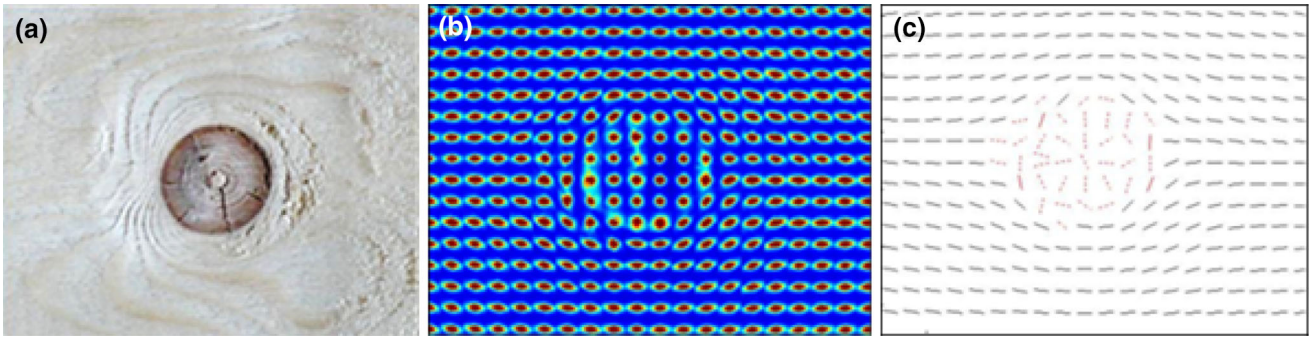

Fig. 2 **a** Wood surface containing a knot; **b** image illustrating the tracheid effect; **c** fibre orientation on the wood surface identified by utilizing the tracheid effect. Reprinted with permission from Petersson (2010)

TRITOP coordinate system, resulting in combined displacement data valid for the whole surface of $132 \times 3{,}710$ mm^2. Oscarsson (2014) thoroughly described the principle of applying the TRITOP system.

2.2 Fibre angle detection using laser scanning and the tracheid effect

A WoodEye scanner from Innovativ Vision AB was used to detect the fibre angles on the board surfaces. Such a scanner is generally equipped with conveyor belts, four sets of multisensor cameras and dot lasers. To detect the fibre orientation on wood surfaces, the scanner utilizes the so-called tracheid effect, i.e. the most extended principal axis of light intensity distribution around a laser dot is oriented in the direction of the fibre. Figure 2 shows an example of how the fibre directions on a wood surface are identified using the tracheid effect. The photograph to the left shows a piece of wood surface including a knot; the middle image shows how the light from dot lasers spreads onto the wood surface and the right plot displays the identified fibre orientation. The local fibre angles on the flat and edge surfaces of a wooden board are registered as a board is fed lengthwise through the scanner. In this study, the resolution employed for the scanned data, i.e. the distance between two laser dots, cf. Figure 2, was set to 1.4 mm in the x-direction and to 3.6 mm in the y-direction (cf. Figure 1b). Nyström (2003) presented a thorough description of the tracheid effect.

2.3 Calculation of a bending MOE profile based on measured displacement information

The displacements corresponding to the load increments between load stages 0 and 2, between stages 0 and 3 and between stages 0 and 4 were utilized to assess local bending stiffness in terms of bending MOE profiles. The calculation procedure can be summarized as follows. For the mentioned load stages (0, 2, 3 and 4), the 3D TRITOP coordinates from the subareas of the examined surface were transferred to MATLAB and based on displacements that occured between load stage 0 and each of the other three load stages, the distribution of corresponding 2D strains in the x- and y-directions and in shear were calculated using MATLAB.

According to the Euler–Bernoulli beam theory, plane cross sections perpendicular to the longitudinal axis of the beam remain plane and perpendicular to the longitudinal axis during deformation. The latter means that no shear deformations are supposed to occur. However, the present study indicates that the position in the board cross section, where zero strain occurs in the x-direction, varied along the board. The y-coordinate of the neutral layer, here denoted $\overline{y}$, is thus a function of x, i.e. $\overline{y} = \overline{y}(x)$. Hence, the sectional bending stiffness EI_z at a particular position along the x-axis can be calculated as

$$EI_z(x) = -M(y - \overline{y})/\epsilon_x \quad (1)$$

where M is the applied bending moment corresponding to the load increment between two load stages and ε_x is the strain in x-direction at a coordinate on the cross section, i.e. $\varepsilon_x = \varepsilon_x(x,y)$. Thus, as long as the beam theory assumption of plane cross sections remaining plane is valid, any detected strain value $\varepsilon_x = \varepsilon_x(x,y)$ and the corresponding distance from the neutral layer may be used to calculate EI_z. Note that the applied bending moment, see Fig. 1a, is here regarded as a positive bending moment, which explains the minus sign in Eq. (1).

Of course, strains in the x-direction that actually appear over cross sections do not perfectly reflect the assumption of plane sections remaining plane during bending and are not distributed exactly as shown in Fig. 1c. Therefore, linear regression is applied on the detected strains over a cross section before Eq. (1) is actually applied to calculating bending stiffness. The position of the neutral layer, $\overline{y}$, is the y-coordinate where the adjusted strain distribution

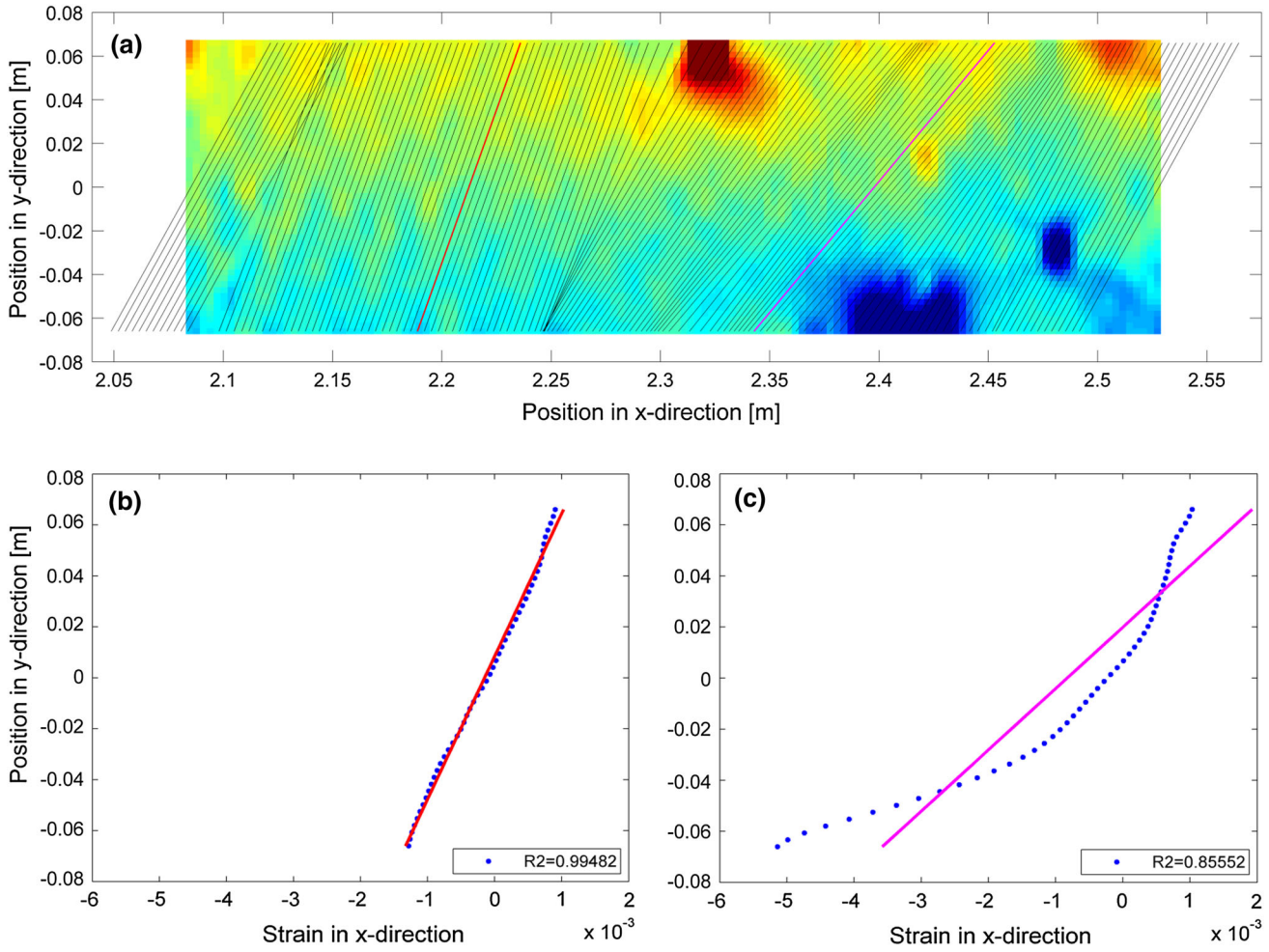

Fig. 3 Example of the implemented linear regression on sections in the *x*-direction based on displacements between load stages 0 and 4 of one ARAMIS project. Key: **a** the *color plot* displays the strain distribution in the *x*-direction with a smoothing function applied. Each value in the strain plot represents an average stain over its surrounding area of 12 × 12 mm^2. Lines of regression are calculated on the basis of strains representing average values over 80 mm in the *x*-direction; two lines of regression are highlighted in *red* and *purple*; **b**, **c** the highlighted *red* and *purple lines* are plotted again along with the strain values on which they are based (*blue dots*). The corresponding R^2 values indicates to what extent the strains over the vertical sections comply with straight lines

based on linear regression achieves the zero value. The colour plot in Fig. 3a shows strains in the *x*-direction. The strains represent average strain values over surrounding areas of 12 × 12 mm^2 and correspond to the deformations occurring between load stages 0 and 4. The inclined straight lines in the same figure represent calculated lines of regression of strains over cross-sections. The strains on which these lines are based on, however, average strains over 80 mm in the *x*-direction. Figure 3b, c shows 80 mm average strains in the *x*-direction (blue dots) and lines of regression calculated on the basis of these values for a section free of knots/defects (Fig. 3b, red line) and for a section of the board with knots (Fig. 3c, purple line). In the knot-free section the strains follow the straight line very well, with a coefficient of determination $R^2 = 0.995$, whereas the strains in the section with knots clearly deviate from the line of regression, with a coefficient of determination $R^2 = 0.856$. The example also shows that the strains represented by an inclination of the regression lines are larger in the section with knots than in clear wood, i.e. the bending stiffness in a defect free section is higher than in a section with knots. The stiffness profile of the entire board is established by considering all the cross sections along the board. The number of such sections is determined by the spatial resolution in the *x*-direction of the measurement data. Finally, the bending MOE profile, $E_b(x)$, is obtained as:

$$E_b(x) = \frac{EI_z(x)}{bh^3/12} \tag{2}$$

where b is the dimension of the board in the z-direction and h in the y-direction.

The fact that cross sections in knotty areas do not in reality remain plane means, of course, that beam theory is not actually valid in a local sense in inhomogeneous parts of the board. Very often when analysing engineering structures the basic assumptions of beam theory are not valid in a local sense but still calculations lead to useful and accurate results on a somewhat more global level. In a local sense it may be questioned to talk about bending stiffness at all, because bending stiffness is a concept that completely relates to beam theory, but on a more global level, say on distances longer than knots or knot clusters, bending stiffness profiles are relevant. The procedure employed herein, utilizing lines of regression, also means that the bending stiffness profiles, even on a local level, are established in a well-defined way.

2.4 Calculation of a bending MOE profile on the basis of scanned local fibre orientation

Olsson et al. (2013) suggested a scheme to calculate a bending MOE profile based on scanned fibre angles of board surfaces and showed that a rather accurate prediction of bending strength is performed based on such MOE profiles. The method is based on fibre angle data obtained through dot laser scanning of all four longitudinal surfaces of boards using a WoodEye scanner. Transformations taking initially assumed material properties in local directions with respect to a wood fibre into account provide the basis for calculation of local bending stiffness in the global x-direction, which in turn is the basis for establishing a bending MOE profile. As in Olsson et al. (2013), many important assumptions were also applied here. Specifically, (1) density, Poisson's ratio and the MOE in the local longitudinal fibre direction E_l are constant within a board; (2) stiffness parameters other than E_l are linear functions of E_l; (3) fibre angles detected on the surfaces are located in the longitudinal–tangential (l–t) plane; (4) the fibres are oriented in a plane that coincides with the wood surfaces, i.e. the so-called diving angle is assumed to be zero; and (5) the fibre angles detected on a surface are representative for the fibre orientation to a certain depth into the board.

The steps taken to calculate the MOE profile using scanned fibre angles can be summarized as follows:

- The fibre angle at each data point on the measured board surface is detected through dot laser scanning and the tracheid effect with a spatial resolution of 1.4 mm in the x-direction and 3.6 mm in the y-direction. An example of such detected fibre orientations in a narrow segment of the board's surface is shown in Fig. 4a. Figure 4a shows a piece of the board's surface consisting of all flat and edge surfaces, denoted 'S1–S4'; the dashed arrow drawn on S1 shows the global x-direction; a small segment with a length marked dx is highlighted with black frame and the corresponding fibre orientations estimated from the tracheid effect within this segment are indicated.
- The assumed material properties are transformed from the local system l-r-t, with the l-axis coinciding with the fibre direction, to global directions, whereby the local material stiffness in the x-direction along the board, $E_x(x, y)$, is obtained. As shown in Fig. 4b, the obtained E_x values represent the segment in Fig. 4a.
- Referring to Fig. 4c, the cross-section is divided into four zones, each with one boundary coinciding with one surface of the board. The sketch to the right is an enlargement of the cross section, which is further divided into small strips, and one strip is highlighted in grey. Hence, by applying assumption (5) mentioned above the transformed E_x is valid for the strip and by summarizing the contributions of all the strips of the cross section, the bending stiffness can be calculated as:

$$EI_z(x) = \iint E_x(y - \overline{y})^2 dA \tag{3}$$

where

$$\overline{y} = \iint E_x y dA \Big/ \iint E_x dA \tag{4}$$

- So far, the calculation is based on a nominal set of material stiffness parameters of which all, in accordance with assumption (2), are linear functions of E_l. To find a true, representative value of E_l for the examined board, a 1-D finite element model with stiffness as a function of x is given by

$$EA(x) = \iint E_x dA \tag{5}$$

The resonance frequency, calculated using the 1-D model, was compared to the frequency measured dynamically in the laboratory, i.e. 637 Hz (cf. Table 1). The value of E_l employed in the model is then adjusted so that the resonance frequency obtained from the model became identical to that assessed experimentally. Therefore, a reasonable value of E_l is determined.
- Finally, the bending MOE profile, $E_b(x)$, is calculated according to Eq. (2).

3 Results and discussions

Figure 5a shows color images of all four longitudinal board surfaces. The surface highlighted and marked as S1 was examined by the DIC system during the bending test. Figure 5b shows the complete strain distribution in the x-direction, estimated on

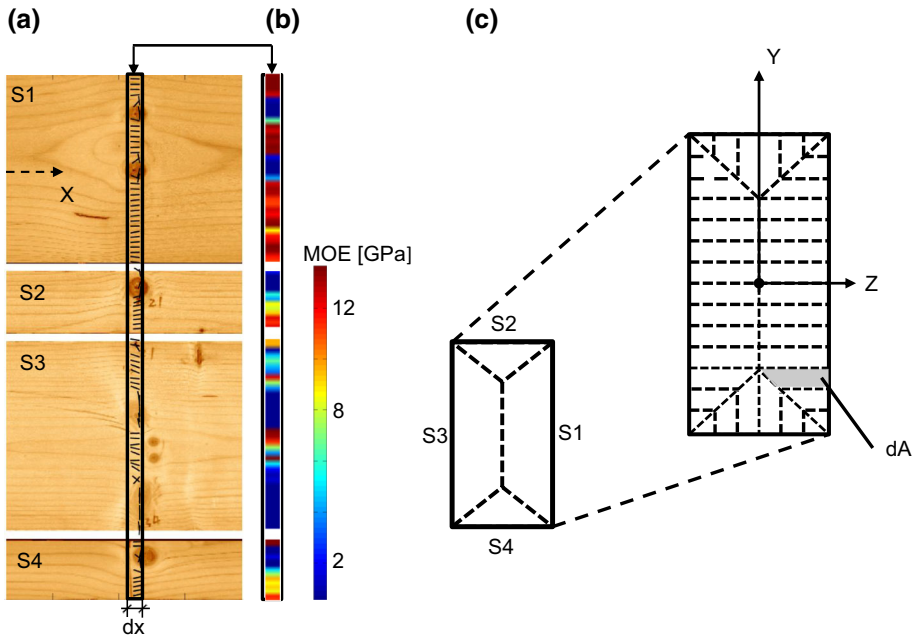

Fig. 4 Illustration of the stiffness integration scheme by Olsson et al. (2013). Key: **a** an image of a piece of the board's surface consisting of all flat and edge surfaces denoted as S1–S4; the *dashed arrow* shows the global *x*-direction; a small segment with a length marked as dx is highlighted with a *black frame* and the corresponding fibre orientations within is indicated. **b** The local E_x variation representing the segment in **a** obtained by the material property transformation using the fibre orientations as indicated in **a**; the color map used for the E_x plot is shown to the *right*. **c** a cross-section of the board showing the sectional stiffness integration principle. The cross-section is divided into four zones, each with one boundary coinciding with one surface of the board. The *sketch* to the *right* is an enlargement of the cross section, which is further divided into small strips, and one strip is highlighted in *grey*, showing that the transformed MOE is valid for the strip

the basis of the deformation between load stages 0 and 4, with the color bar to the right showing the strain levels. Strains displayed in this color plot are average values over the surrounding area of 12×12 mm^2. Figure 5c shows the bending MOE profiles calculated on the basis of strains as described above. The E_b values displayed by the curves are calculated from average sectional strains over a length of 80 mm in the *x*-direction, i.e. the E_b values displayed at each position, x, depend on the strains shown in Fig. 5b over an area $x \pm 40$ mm, -66 mm $< y <$ 66 mm. Three different curves plotted in different colors are displayed, representing the E_b variation calculated on the basis of the strains developed between load stages 0 and 2 (red line), between load stages 0 and 3 (black line) and between load stages 0 and 4 (green line). From Table 2, note that the measurement of the 12 ARAMIS projects were carried out in a sequence, for load stages 0, 2 and 4, from lower to higher *x*-coordinates and for load stage 3 in the opposite direction (cf. Fig. 1a, b).

The image shown in Fig. 5a shows numerous knots in the examined board. If smaller knots, such as pin knots, are disregarded, the remaining larger knots are grouped into a number of clusters scattered along the *x*-direction and any sections between are more or less free from knots. The strains presented in Fig. 5b clearly show that the lower and upper edges of the board are exposed to tension (lower) and compression (upper). When comparing the strain distribution to the board images, strain concentrations at knots emerge very clearly. Furthermore, some strain concentrations are also located where no knots are visible on the examined surface S1, but on other surfaces at the same position in the *x*-direction. This effect is observed on both the tension and compression sides of the board, e.g. at $x = 2.5$ m. Therefore, knots may influence the strain distribution of surface S1, even if they are not visible on this surface of the board. Hence, with exception of a very local scale, i.e. on the level of a single knot, the deformation of the board in the *xy*-plane is well described by the strains detected on only one of the flat surfaces.

The three E_b profiles shown in Fig. 5c, representing different load levels, agree well with each other, i.e. stable results are obtained from the DIC measurements. Since the E_b profiles exhibited in Fig. 5c are more or less identical, irrespective of measurement sequence direction (see Table 2), it is concluded that any possible creep that occurs during implementation of the 12 ARAMIS projects at each load stage is so low that it can be disregarded. Moreover, the bending MOE profiles reveal that the stiffness of the most unfavorable section, which coincides of course with knots and knot cluster, may drop to less than 30 % of the

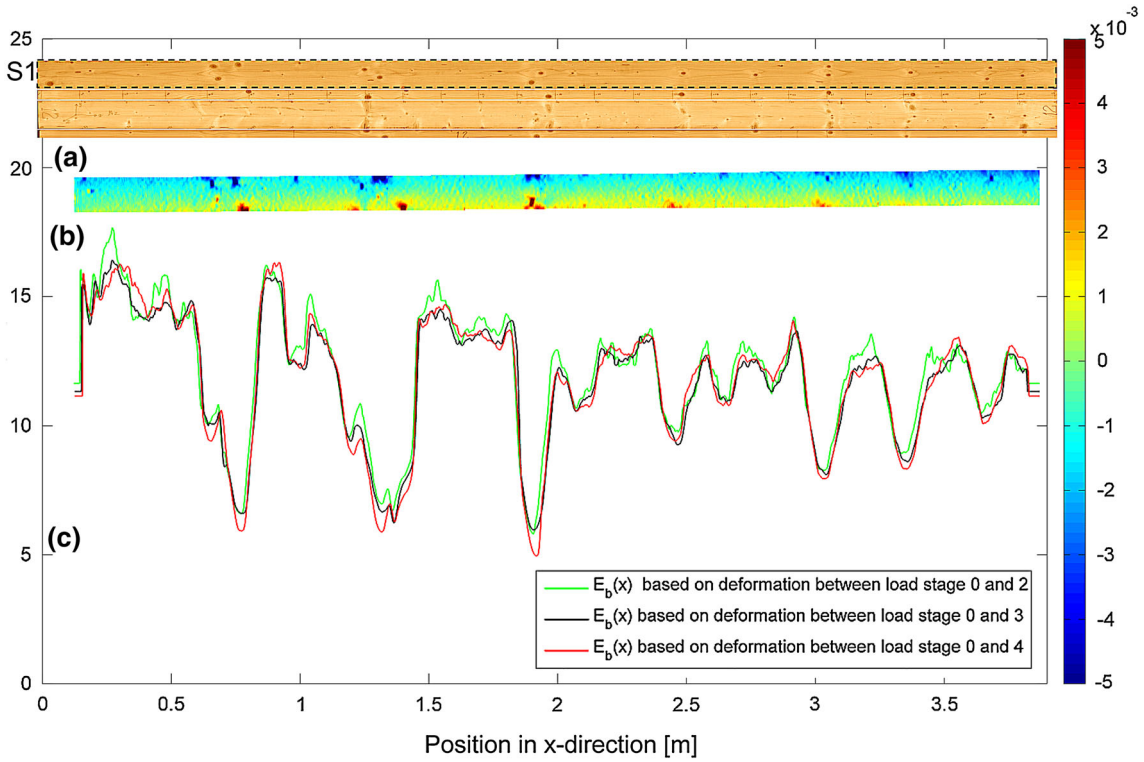

Fig. 5 Results from the DIC measurement. Key: **a** surface image of the board; the surface marked as S1 was examined by the DIC-system. **b** Detected strain distribution in the *x*-direction on surface S1 corresponding to the load increment applied between load stages 0 and 4. **c** Three estimated E_b profiles calculated on the basis of strain fields corresponding to different pairs of load stages

stiffness in a defect-free section. As well, weak sections where drops appear in the curves have a typical length of about 200 mm. There is a decreasing trend, from left (the top end) to right (the root end) of the board, for the MOE value in knot free sections. This indicates an MOE variation for clear wood within this particular board. Lundström et al. (2007), for example, have pointed out that a more or less systematic MOE variation for clear wood along a stem may occur due to a number of factors related to the growth conditions of the tree.

Figure 6a shows E_b profiles calculated on the basis of detected fibre angles from laser scanning (blue lines) along with an E_b profile based on DIC measurements (red line). All the profiles represent moving average values over a length of 80 mm along the board. The moving average length is the same one as was used by Olsson et al. (2013). It is not very sensitive if moving average values are calculated over a somewhat smaller or longer distance but, of course, shorter lengths lead to larger variations and longer lengths lead to smaller variations in the curve, see Olsson et al. (2013) and Oscarsson (2014). Note that two different blue curves are drawn, one lighter than the other. They both represent MOE profiles based on scanned fibre angles, and almost coincide. Whereas the MOE profile drawn in light blue represents the average E_b of all n sections (each denoted $E_{b,i}$, where i is a number between 1 and n) that fit within an 80 mm distance in the x-direction, as Olsson et al. (2013), the darker blue line represents the reversed average of the inverted $E_{b,i}$ of the n sections included. The E_b profile represented by the light blue line is thus calculated as

$$E_b(x) = \frac{E_{b,1} + E_{b,2} + \ldots + E_{b,n}}{n} \tag{6}$$

while the E_b profile represented by the darker blue line is calculated as

$$E_b(x) = \frac{1}{\left(\frac{1}{E_{b,1}} + \frac{1}{E_{b,2}} + \ldots + \frac{1}{E_{b,n}}\right)/n} \tag{7}$$

Note that the red line representing the E_b profile, based on detected strains for the load increment between load stages 0 and 4, is calculated in a way corresponding to Eq. (7). The profile would have been very sensitive to measurement noise if it was calculated in accordance with Eq. (6), since a single section with strains seemingly close to zero would then result in a large overestimation of the MOE. The horizontal red line drawn in Fig. 6a indicates a constant level of 11.8 GPa representing the average value of the red E_b profile, the horizontal blue line indicates a constant level of 11.4 GPa representing the average value

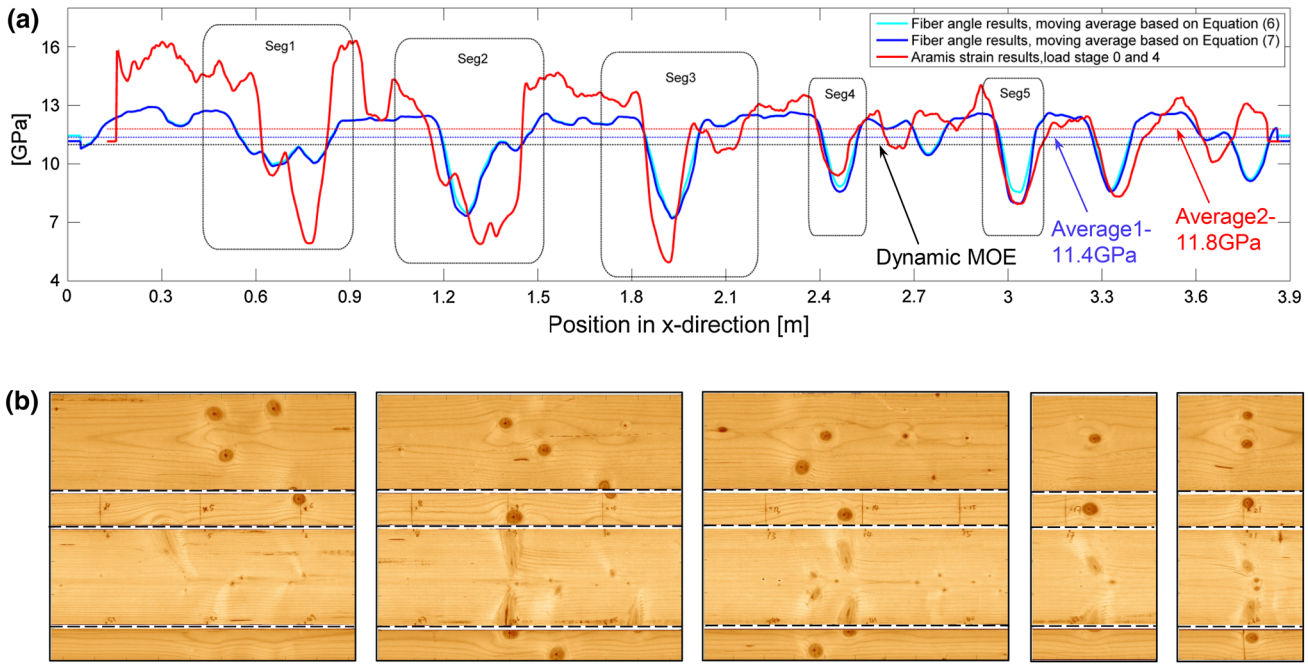

Fig. 6 Diagrams of the estimated E_b profiles based on fibre angles (*blue curves*) and strains detected by DIC technique for the load increment between load stages 0 and 4 in the bending test (*red curve*), respectively, and images of the actual board surfaces. Key: **a** the estimated E_b profiles having a moving average length of 80 mm. **b** The surface images of five chosen segments (*encircled* in **a**) placed in the order of their positions along the *x*-direction

of the dark blue E_b profile and the horizontal black line indicates the direct dynamic MOE received from axial dynamic excitation and weighing of the board (10.98 GPa). The model represented by the blue curves is calibrated in accordance with the first axial eigenfrequency and therefore it is not surprising that the average MOE of this model is close to the dynamic MOE. However, it is somewhat surprising that the average MOE of the bending stiffness curve based on static four point bending and detected strains, i.e. the red curve, is higher than the dynamic MOE. Normally, dynamic MOE is slightly higher than static MOE. Figure 6b shows color images from parts of the board that are marked as segments 1–5 in Fig. 6a.

The tendency that E_b in clear wood is higher at the left end of the board than the right, shown by the profile based on strain fields from DIC measurements, is not shown by the profile based on fibre angle information. Of course, this is a consequence of the basic assumption made in the calculation model based on fibre angles, namely that E_l is constant within the board. Thus, the comparison between the two profiles reveals, in this respect, a deficiency of the method suggested by Olsson et al. (2013).

When comparing the bending MOE profiles with respect to the occurrence of weak sections due to knots and clusters of knots along the board, the positions are highly correlated, since drops in the two curves appear at about the same *x*-positions along the board. Regarding the level of the drops, some parts of the profiles agree very well and some do not. When comparing the weak sections highlighted in Fig. 6, viz. segment 1 to segment 5, the reduction of bending MOE obtained for segment 4 and segment 5 in the right part of the board agrees very well. The knot clusters in these segments are concentrated to a narrow band in the *x*-direction and spread only in the *y*-direction. The knot cluster of segment 1, segment 2 and segment 3 are more dispersed in the *x*-direction; for these knot clusters the profile based on fibre angle information seems to substantially underestimate the local decrease in bending stiffness. The question of why the same reduction in E_b is shown by the different profiles for knot clusters concentrated to a narrow band in the *x*-direction, but not for knot clusters dispersed in the *x*-direction should be sought in the basic assumptions from the calculation model based on fibre angle information and integration of bending stiffness over board cross sections. This is done below.

Shear strains and normal strains in the *y*-direction, like normal strains in the *x*-direction, can be calculated from displacements detected by DIC measurements. Figure 7 shows images of surface S1 (cf. Fig. 5) of the board for two of the segments defined in Fig. 6, i.e. for segment 2 and segment 5, with normal strain fields in the *x*- and *y*-directions and shear strain fields in the *xy*-plane. The strain fields may be used to verify to what extent the assumption of the beam theory is valid on a local level in the board for two different patterns of knot clusters, i.e. knots dispersed in the *x*-direction (segment 2) and knots being concentrated to a

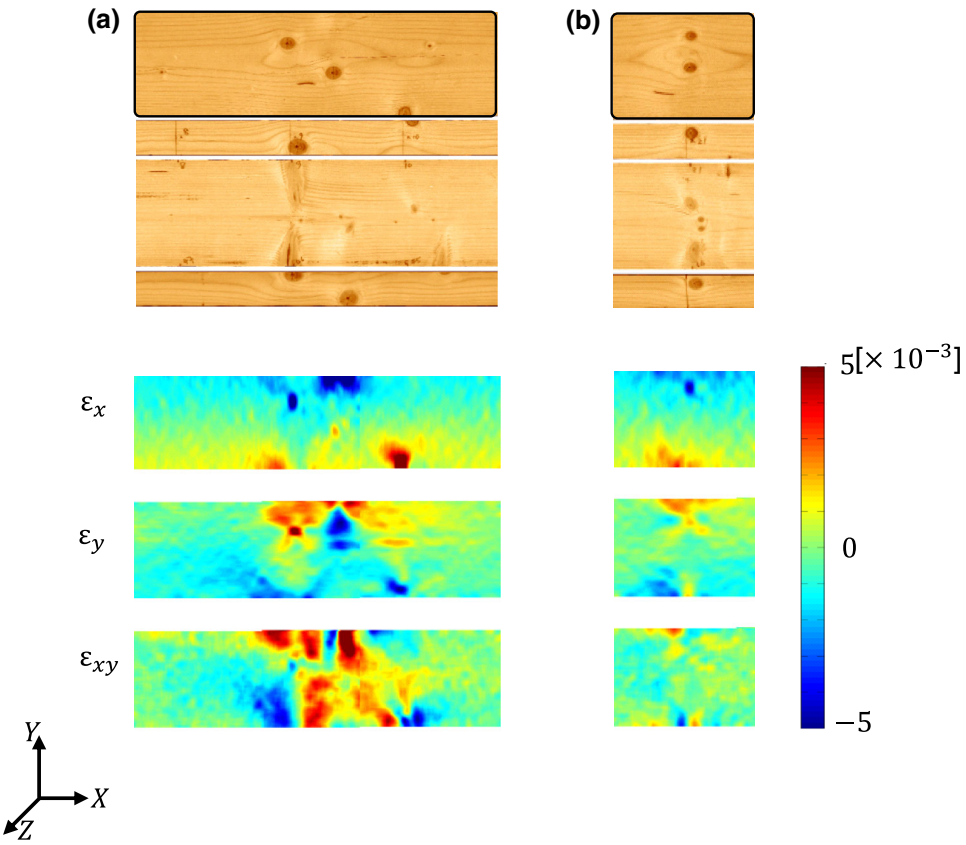

Fig. 7 Surface image and strain fields in *x*- and *y*-direction and in shear, of segments no. 2 and 5

narrow band in *x*-direction (segment 5). The Euler–Bernoulli beam theory assumes that the only type of strains present in the beam is normal strain in the *x*-direction. Strains shown in Fig. 7, however, clearly show that shear strains and normal strains in the *y*-direction occur in the material, though the board was subjected to a pure bending moment. The shear strains and normal strains in the *y*-direction are large within the knot cluster of segment 2, where the knots are dispersed, but moderate within the knot cluster of segment 5. The constraints applied by the beam theory regarding deformations in the material, therefore, lead to a substantial overestimation of the local stiffness in segments where knot clusters as in segment 2 are present. For knot clusters of the type present in segment 5, on the other hand, the applied beam theory implies no severe restrictions on deformations compared to those actually present. Therefore, it is not surprising that the local bending stiffness calculated on the basis of detected fibre angles is in good agreement with the local bending stiffness calculated on the basis of the strains in the *x*-direction from DIC measurements.

4 Conclusion

In this study, the possibility to assess the local variation in bending MOE along a board based on high resolution displacement data, determined at different load stages by means of DIC technique, was investigated. MOE profiles established on the basis of different load levels were almost identical and the result is thus regarded as stable and reliable. The MOE profiles illustrate weak sections along the board, due to the presence of knots and knot clusters, in the form of local drops in the curve. For the investigated board, the weak sections are typically about 200 mm long in the board direction and the local bending stiffness of the weakest section decreases to less than 30 % of the stiffness of the defect-free sections. The profile also shows that the MOE of clear wood at one end of the examined board (the top end) is substantially larger than at the other end (the root end).

A bending MOE profile was also established on the basis of local fibre orientation data from laser scanning of the board surfaces and a calculation model based on integration of bending stiffness over board cross sections. Establishing the profile in this manner shows good agreement with the profile established on the basis of displacements detected by the DIC systems. The two different bending MOE profiles show close agreement regarding positions where weak sections appear. For some of these positions the magnitudes of the drops in the profiles also agree. However, for other weak sections substantial discrepancies were found when the magnitudes of the drops in

the two MOE profiles are compared. This lack of agreement is mainly related to the pattern of the corresponding knot clusters in the board and the assumptions employed in the calculation model. For knot clusters where the knots are located close together in the *x*-direction of the board, the deformation can be properly predicted by the method developed by Olsson et al. (2013). Yet, in regions where knots are dispersed in the *x*-direction, these assumptions place serious restrictions on the deformation in the material that do not correspond to the actual deformation taking place. Thus, where knot clusters are dispersed in the *x*-direction, the calculation model overestimates the local bending stiffness.

Overall, the present research supports conclusions drawn in previous research, that reasonably accurate bending MOE profiles can be established on the basis of fibre orientation information in the way described. Because it is also known that the strength of wood is strongly correlated to localized MOE, this research also supports that such profiles may be used to more accurately predict timber strength than other methods in use. However, the findings of the present study provide a basis for further improvements of the grading methods based on knowledge of localized MOE. Finally, it should be stressed that detailed strain fields obtained for a whole wooden board based on the DIC technique may be of great interest whenever theoretical models for wood, intended to be applied to timber, are to be evaluated and calibrated. Models to be examined with the support of such information may, for example, involve grain-flow analogies, plasticity, micro-mechanical approaches and fracture mechanics.

Conflict of interest The authors declare that they have no conflict of interest.

References

Hu M, Johansson M, Olsson A, Bengtsson C, Brandt A (2011) Grading of sawn timber using the vibration technique—locating imperfections based on flexural mode shapes. In: Divos F Proceedings of the 17th international nondestructive testing and evaluation of wood symposium, 1, University of West Hungary, Sopron Hungary, September 14–16, pp 269–276

Lundström T, Heiz U, Stoffel M, Stöckli V (2007) Fresh-wood bending: linking the mechanical and growth properties of a Norway spruce stem. Tree Physiol 27(9):1229–1241

GOM mbH (2007) ARAMIS user manual—software, version 6.1

Nyström J (2003) Automatic measurement of fibre orientation in softwoods by using the tracheid effect. Comput Electron Agric 41(1):91–99

Olsson A, Oscarsson J, Serrano E, Källsner B, Johansson M, Enquist B (2013) Prediction of timber bending strength and in-member cross-sectional stiffness variation on the basis of local wood fibre orientation. Eur J Wood Prod 71(3):319–333

Orosz I (1976) Relationship between apparent modulus of elasticity, gauge length, and tensile strength of timber. Wood Sci Technol 10(4):273–291

Oscarsson J (2014) Strength grading of structural timber and EWP laminations of Norway spruce—development potentials and industrial applications. Doctoral dissertation, Department of Building Technology, ISBN: 978-91-87427-84-8, Linnaeus University, Växjö, Sweden

Petersson H (2010) Use of optical and laser scanning techniques as tools for obtaining improved FE-input data for strength and shape stability analysis of wood and timber. In: Proceedings of the IV European conference on computational mechanics, Paris, May 16–21

Sjödin J, Serrano E, Enquist B (2006) Contact-free measurements and numerical analyses of the strain distribution in the joint area of steel-to-timber dowel joints. Holz Roh Werkst 64:497–506